ACS NANOSCIENCE Au
AN OPEN ACCESS JOURNAL OF THE AMERICAN CHEMICAL SOCIETY

pubs.acs.org/nanoau

Perspective

Intermetallic Nanoarchitectures for Efficient Electrocatalysis

Ho Young Kim,[#] Minki Jun,[#] Sang Hoon Joo,* and Kwangyeol Lee*

Cite This: https://doi.org/10.1021/acsnanoscienceau.2c00045

Read Online

ACCESS | Metrics & More | Article Recommendations

ABSTRACT: Intermetallic structures whose regular atomic arrays of constituent elements present unique catalytic properties have attracted considerable attention as efficient electrocatalysts for energy conversion reactions. Further performance enhancement in intermetallic catalysts hinges on constructing catalytic surfaces possessing high activity, durability, and selectivity. In this Perspective, we introduce recent endeavors to boost the performance of intermetallic catalysts by generating nanoarchitectures, which have well-defined size, shape, and dimension. We discuss the beneficial effects of nanoarchitectures compared with simple nanoparticles in catalysis. We highlight that the nanoarchitectures have high intrinsic activity owing to their inherent structural factors, including controlled facets, surface defects, strained surfaces, nanoscale confinement effects, and a high density of active sites. We next present notable examples of intermetallic nanoarchitectures, namely, facet-controlled intermetallic nanocrystals and multidimensional nanomaterials. Finally, we suggest the future research directions of intermetallic nanoarchitectures.

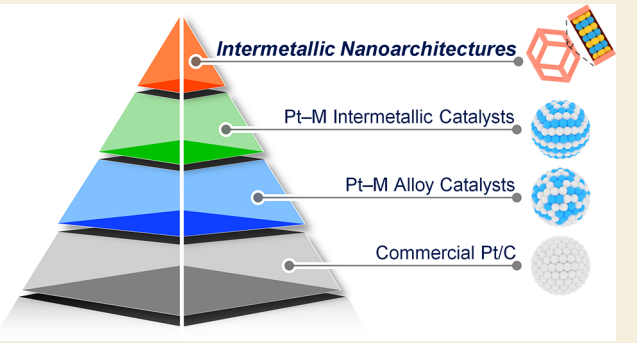

KEYWORDS: *Intermetallics, Nanoarchitectures, Electrocatalysis, Active sites, Energy conversion reactions*

INTRODUCTION

With increased attention being paid to carbon neutrality, renewable energy conversion systems such as fuel cells and electrolyzers have garnered a great deal of interest.[1−3] These electrochemical devices that utilize small molecule transformation reactions empower efficient energy production in a clean and sustainable manner. Over the past decades, the ever-increasing demand for the renewable energy-driven hydrogen economy has triggered the development of efficient electrocatalysts. Currently, platinum-group metal (PGM)-based multimetallic electrocatalysts are at the forefront of the associated industry. The multimetallic composition can reduce the contents of expensive PGMs and engender strain and ligand effects onto the PGM surface, leading to a higher intrinsic activity per each active site than PGM monometallic catalysts.[4,5]

Among the diverse types of multimetallic catalysts, intermetallic structures have emerged as a novel class of advanced electrocatalysts.[6−11] Their long-range ordered atomic arrays with constant stoichiometry and well-defined crystal structure induce catalytic properties, which are distinct from the alloy (solid solution) phase of random atomic arrangement with the same composition. For example, in the case of the A−B bimetallic system, its intermetallic phases have strong A−B bonds, whose bonding strength is much higher than the average of A−A and B−B bonds, leading to high stability than random alloy phases by preventing the leaching of each metal species. In addition, the ordered atomic arrays maximize the number of A−B bonds, intensifying the ligand effect induced by the interatomic partial charge transfer. The intensified ligand effect can boost catalytic activity by increasing the population of surface sites that have optimal binding strengths with reaction intermediates.[11] Furthermore, the alterations in A−B bond length or repeating arrangements (crystal structure) can modulate the binding strength between the reaction intermediates and catalytic surfaces by the intensified strain effect, accelerating the reaction kinetics and improving the selectivity toward high-value products. Inspired by their remarkable activity, stability, and selectivity, enormous efforts to synthesize efficient intermetallic catalysts have been made.[6−10] In the 1990s, most intermetallic catalysts were prepared by thermal annealing of random alloy catalysts at elevated temperatures. However, the prepared catalysts often showed large agglomerates with uneven size distribution and irregular shape due to a lack of insight into the suppression of nanoparticle (NP) sintering. In addition, crucial factors for preparing intermetallic phases, such as synthetic temperature

Received: September 2, 2022
Revised: October 20, 2022
Accepted: October 20, 2022

and composition ratio, were not firmly established, resulting in low phase purity.[12]

Since the 2010s, a rapid progress has been made in the design of high-performance intermetallic catalysts with controlled size and shape (Figure 1). Nazar and co-workers

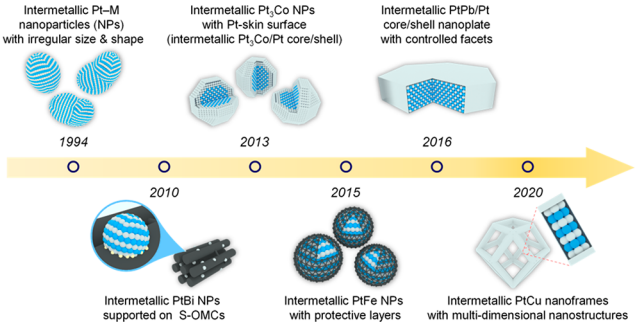

Figure 1. Timeline for the advances in intermetallic nanocatalysts. Intermetallic nanoarchitectures with controlled size and well-defined shape, including intermetallic nanocrystals with controlled facets and multidimensional nanostructures, represent advanced intermetallic nanocatalysts.

developed intermetallic PtBi NPs with a size of 1.5 nm using sulfur-coated ordered mesoporous carbon (S-OMC) as carbon support.[13] The S atoms in S-OMC trap metal precursors, assisting in the size reduction of intermetallic NPs. In 2013, the Abruña Group synthesized intermetallic Pt_3Co/Pt core/shell structures with a precise composition ratio using a simple impregnation-reduction method.[14] In this synthesis, the adoption of the precise composition was effective in obtaining highly crystalline intermetallic phases, guiding follow-up studies. Owing to the three atomic-layer-thick Pt shells (Pt-skin), the prepared catalyst demonstrated enhanced ORR activity and durability compared to the alloy counterpart. Next, several research groups have developed protective layer-mediated annealing methods to achieve uniform size distribution in intermetallic NPs.[15−17] The uniform spherical intermetallic NPs exhibited enhanced activity and durability compared to the irregular NPs. The key to these strategies is encapsulating individual alloy NPs with protective layers before the high-temperature annealing step to mitigate the inter-particle diffusion. Thermally stable SiO_2, MgO, and carbon-shell have been found suitable as protective layers. More importantly, the intermetallic nanoarchitectures, which refer to intermetallic catalysts with uniform size and controlled shape in nanoscale, have demonstrated unprecedented enhancement in catalytic performances.[11,18−27] Nanoarchitectures, including facet-controlled nanocrystals and multidimensional nanostructures, often expose well-defined crystallographic planes or highly strained surfaces from curved planes, undercoordinated defects, and grain boundaries. These structural features of intermetallic nanoarchitectures engender different binding strengths of reaction intermediates from typical intermetallic NPs, boosting catalytic performance. The remarkable performance enhancement by intermetallic nanoarchitectures triggered several important efforts to comprehend the information about the synthesis and catalytic application of intermetallic catalysts.[6−11] However, their structural impacts of well-defined shape on catalysis have not been discussed in depth. In addition, establishing synthetic strategies for intermetallic nanoarchitectures remains a formidable challenge.

In this Perspective, we introduce recent advances in high-performance intermetallic nanoarchitectures. First, we highlight that the well-defined size, shape, and dimension of nanoarchitectures lead to superior catalytic properties over-simple NPs. We then discuss the inherent structural factors of nanoarchitectures, including controlled facets, surface defects, strained surfaces, and nanoscale confinement effects. We next introduce notable endeavors that boosted the intrinsic activity of intermetallic catalysts by designing facet-controlled intermetallic nanocrystals and multidimensional nanomaterials. Finally, we conclude this Perspective by providing a summary and future research directions for intermetallic nanoarchitectures.

CATALYTIC BENEFITS OF GENERATING NANOARCHITECTURES

It is instructive to discuss the catalytic benefits of nanoarchitecture before presenting the advances in intermetallic nanoarchitectures. It is well-documented that the nanoarchitectures such as nanopolyhedra, nanowires (NWs), nanosheets, and hollow skeletal nanomaterials often show superior catalytic activity over spherical NPs.[4,5] This activity enhancement emanates from the combination of multiple advantages of nanoarchitectures (Figure 2). At first, the

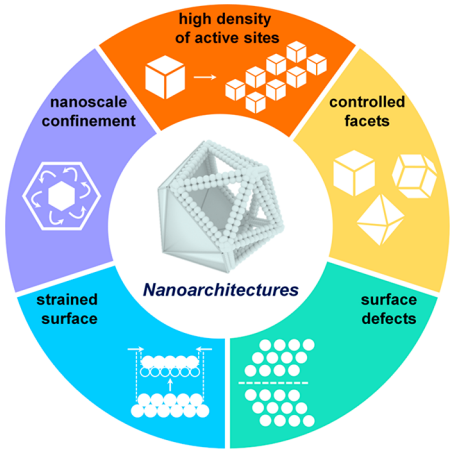

Figure 2. Schematic illustration showing catalytic benefits of generating nanoarchitectures. Synthesizing intermetallic nanoarchitectures can boost the catalytic activity, stability, and selectivity of intermetallic phases by exploiting these advantages.

nanoarchitectures exhibit a higher density of active sites than spherical NPs. In geometry, the solid figure with the smallest surface area at a given volume is a sphere, according to the isoperimetric inequality in three-dimensional (3D) space.[28,29] It implies that when the usage of metal elements is the same, generating nanoarchitectures offers a higher number of active sites by exposing a higher proportion of catalytic surfaces.

Beside the high density of active sites, the sophisticated morphology of nanoarchitectures inherently produces crucial impacts on the catalytic properties of surfaces. For example, nanopolyhedra terminated with well-defined surfaces, such as the cube with (100), the rhombic dodecahedron with (110), and the octahedron with (111) facet, enabled tailoring of catalytic properties via shape control. As the nanoscale embodiment of single-crystalline model catalytic surfaces, these nanoarchitectures provided an opportunity to systematically explore the impacts of controlled facets on catalytic

https://doi.org/10.1021/acsnanoscienceau.2c00045
ACS Nanosci. Au XXXX, XXX, XXX−XXX

Table 1. ORR Performances of Representative Intermetallic Nanoarchitectures along with the Commercial Pt/C Catalyst

catalyst	electrolyte	ECSA[a] ($m^2\ g_{Pt}^{-1}$)	$MA_{0.9\ V}$[b] (A mg_{Pt}^{-1})	$SA_{0.9\ V}$[c] (mA cm_{Pt}^{-2})	ref
Pt/C (TKK)	0.1 M $HClO_4$	77.8	0.3	0.4	
PtPb nanoplates/C	0.1 M $HClO_4$	55.0	4.3	7.8	18
fct-Pt−Co@Pt/C	0.1 M $HClO_4$	30.8	2.8	9.2	20
fct-PtFeIr/C	0.1 M $HClO_4$	84.6	2.0	2.4	22
Pd_3Pb UPINs/C	0.1 M KOH	50.1	0.6	1.2	24
O-PtCuNF/C	0.1 M $HClO_4$	52.7	2.5	4.7	25

[a]electrochemically active surface area. [b]mass activity at 0.9 V vs reverible hydrogen electrode (RHE). [c]specific activity at 0.9 V vs RHE.

activity and selectivity. The catalytic properties of facet-controlled nanocrystals depend on the crystallographic planes of terminated surfaces because each plane has different binding energies of reaction intermediates, even if the reaction and catalyst composition are the same. It stems from distinctions in the surface coverage of adsorbate and the coordination number by an intrinsic difference in the atomic packing for the crystal planes.[28,29]

In addition, when nanoarchitectures have a more complex morphology or polycrystalline nature, their surfaces terminate with high-index planes comprising abundant defects, including steps, kinks, and grain boundaries.[28−31] The defective surfaces strongly interact with adsorbate due to their high surface energy, influencing reaction pathways. Furthermore, in the cases of multidimensional nanomaterials beyond the solid nanocrystals, the surface of nanoarchitectures becomes concave or convex in a considerable proportion. Since these curved surfaces contain significant lattice mismatches, the intense strain effects are imposed on the surface of multi-dimensional nanoarchitectures, leading to fine-tuning the electronic structures of catalysts. Collectively, the geometric features inherent in the surface of multidimensional nano-structures can serve as highly energetic surface sites, tuning the surface electronic structures and inducing superior intrinsic catalytic activity over solid NPs.[28−31] Moreover, the hollow skeletal nanomaterials boost the intrinsic activity of catalytic reactions by the nanoscale confinement effect. Within these 3D nanoarchitectures, the reactant molecules undergo multiple effective collisions via Knudsen diffusion to activate the reactions.

These structural advantages of nanoarchitectures can be combined with the unique catalytic properties of intermetallic structures to generate efficient electrocatalysts, as demonstrated by the enhanced activity of intermetallic nano-architectures for ORR, which is the most utilized as a probe reaction (Table 1).

FACET-CONTROLLED INTERMETALLIC NANOCRYSTALS

First, we present the notable exemplars of facet-controlled intermetallic nanocrystals and their synthetic strategies.[18−21] We focus on the enhancement in cataytic activity, stability, and selectivity of intermetallic nanoarchitectures, which are aroused by terminating the surfaces of intermetallic structures with well-defined crystallographic planes. The wet-chemical approach, a powerful method for preparing shape-controlled nanocrystals, enables the bottom-up synthesis of facet-controlled intermetallic nanocrystals.[6−10,18,19] The successful preparation of the intermetallic nanocrystals with well-defined shapes rests on the judicious selection of structure directing agents. In addition, the reaction rate should be controlled to induce a simultaneous occurrence of particle growth in specific directions and the atomic ordering. Hence, mild reducing agents are favored to lower the reaction rate in a controllable manner.

In a notable example, Huang and co-workers synthesized highly uniform hexagonal nanoplates constructed with intermetallic PtPb core and Pt shell (PtPb nanoplates) using a mixture of oleylamine (OAm) and 1-octadecene as structure directing agents and ascorbic acid (AA) as a reducing agent (Figure 3a).[18] The prepared PtPb nanoplates exhibit an anisotropic intermetallic PtPb core that has {010} surfaces at the edges and {001} surfaces at the top and bottom. Onto the core, the Pt{110} shells are covered (Figure 3b). The weak reducing power of AA was found to be the most crucial factor for constructing well-defined hexagonal plates. AA triggers a

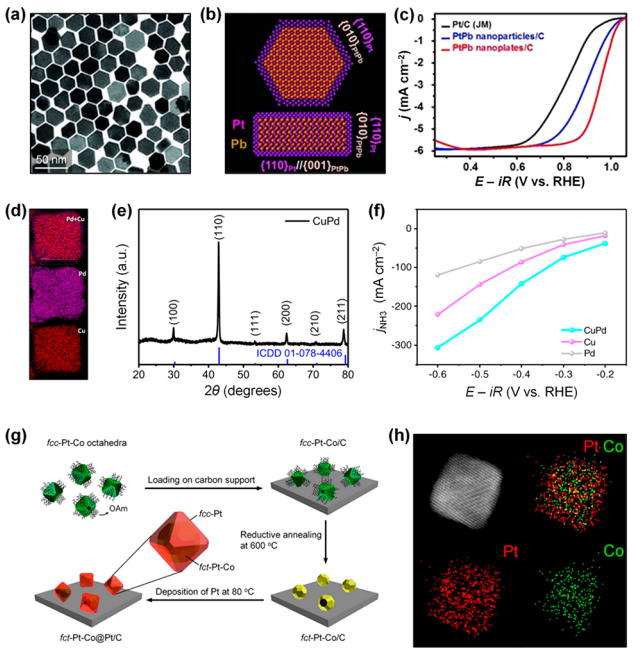

Figure 3. (a) TEM image of PtPb nanoplates. (b) Schematic atom models of the PtPb nanoplate showing the top [(110)Pt//(100)PtPb] and the side [(110)Pt//(001)PtPb] interfaces. (c) ORR polarization curves of PtPb nanoplates/C, PtPb nanoparticles/C, and Pt/C. Reprinted with permission from ref 18. Copyright 2016 American Association for the Advancement of Science (AAAS). (d) EDS elemental mapping data of CuPd nanocubes. (e) XRD patterns of CuPd nanocubes. (f) Current densities for NH_3 production of CuPd nanocubes, Cu nanocubes, and Pd nanocubes. Reprinted with permission under a Creative Commons Attribution 4.0 International License from ref 19. Copyright 2022 Springer Nature. (g) Schematic illustration for the synthesis of *fct*-Pt−Co@Pt/C catalyst. (h) HAADF-STEM image and EDS elemental mapping data of *fct*-Pt−Co@Pt/C catalyst. Reprinted with permission from ref 20. Copyright 2021 American Chemical Society (ACS).

https://doi.org/10.1021/acsnanoscienceau.2c00045
ACS Nanosci. Au XXXX, XXX, XXX−XXX

slow reduction of metal precursors, enabling the interdiffusion and the reorganizing atomic arrays of Pt and Pb atoms simultaneously. Subsequently, the Pt shells are deposited onto the intermetallic PtPb core by slow reduction of remaining Pt ions in the reactant solution. In catalysis, the PtPb nanoplates demonstrated much higher oxygen reduction reaction (ORR) activity than intermetallic PtPb spherical NPs and commercial Pt/C catalysts (Figure 3c). We emphasize that assembling an intermetallic PtPb phase into a facet-controlled hexagonal nanoplate covered by well-defined Pt shells is crucial for performance enhancement. Since the distances between two adjacent atoms in the edge, top, and bottom plane of PtPb core are larger than the Pt{110} planes, significant tensile strain effects are imposed biaxially on the Pt topmost layers. These biaxial tensile strain effects weaken oxygen binding energy on the Pt{110}, boosting the intrinsic ORR activity.

As an another example, Zhu and co-workers designed intermetallic CuPd nanocubes catalyzing nitrate reduction reaction (NO_3RR).[19] For the NO_3RR, Cu (100) surface is a highly selective catalytic surface toward NH_3 formation as shown by the previous single crystal-based studies. In this work, the theoretical calculations of catalyst composition assisted by machine learning predicted that NH_3 production is more favored on the CuPd (100) surfaces than Cu (100) surface. Following the theoretical prediction, CuPd intermetallic nanocrystals terminated with (100) facets were synthesized by heating a mixture of $Cu(acac)_2$, $PdCl_2$, OAm, and trioctylphosphine at 250 °C for 30 min. The prepared CuPd nanocubes exhibit a uniform distribution of Pd and Cu (Figure 3d). As shown in Figure 3e, the X-ray diffraction (XRD) pattern of the intermetallic CuPd nanocubes corroborates the formation of a highly crystalline CuPd intermetallic structure with a body-centered cubic (*bcc*) crystal structure (B2 phase). In this synthesis, the reaction condition with mild reducing power induced a successive decomposition and reduction of $Cu(acac)_2$ and $PdCl_2$. At the early reaction stage, Cu-based NPs are formed first, serving as seeds for Pd nucleation. The generated CuPd nanocrystal grew via multiple processes of galvanic replacement combined with the nanoscale Kirkendall effect, resulting in intermetallic CuPd nanocubes. In the electrochemical test, the intermetallic CuPd nanocube catalysts exhibited a higher NO_3RR current density than Cu and Pd nanocubes, consistent with the theoretical prediction (Figure 3f). Furthermore, the faradaic efficiency for NH_3 production reached 92.5% at −0.5 V vs RHE.

Although the wet-chemical approach is efficient for creating intermetallic nanoarchitectures, the use of mild reducing agents often suffers from overcoming the difference in reduction potentials between two elements, restricting the range of viable compositions for generating intermetallic phases. In addition, the wet-chemical synthesis has an inherent issue in scale-up.[6,9,10] In contrast, the thermal annealing method is usually carried out above 500 °C in a reductive atmosphere, limiting the precise control over the size and shape of catalyst particles. Nevertheless, this useful method allows a broad range of compositions by offering sufficient driving forces to induce the disorder-to-order transformation. Considering the practical applicability, thermal conversion of random alloy nanoarchitectures into their intermetallic counterparts is also effective. For example, Xia et al. developed octahedral nanocrystals comprising an intermetallic Pt−Co core with a face-centered tetragonal (*fct*) crystal structure ($L1_0$ phase) and Pt shell terminated with {111} facets of three to four atomic layers (*fct*-Pt−Co@Pt/C).[20] Briefly, alloy Pt−Co octahedral nanocrystals were synthesized by the colloidal method and supported on carbon black (Figure 3g). Then, the alloy Pt−Co octahedral nanocrystals (*fcc*-Pt−Co/C) with a face-centered cubic crystal structure were annealed at 600 °C for 4 h to form Pt−Co intermetallic nanocrystals (*fct*-Pt−Co/C). This annealing step induced the disorder-to-order transformation and deformed the shape of nanocrystals into a truncated octahedron. Then, the aqueous dispersion of *fct*-Pt−Co/C was mixed with citric acid, and the K_2PtCl_4 solution was added into the mixture at 80 °C to form Pt shells on the surface of *fct*-Pt−Co/C, resulting in *fct*-Pt−Co@Pt/C catalyst. The scanning transmission electron microscopy (STEM) image and corresponding energy dispersive X-ray spectroscopy (EDS) elemental mapping data of *fct*-Pt−Co@Pt/C show a highly ordered intermetallic core and a smooth Pt shell (Figure 3h). The successful production of intermetallic octahedral nanocrystals with well-controlled surface structures unraveled the effects of both interior crystal structure and exterior facets on ORR activity. In the ORR test, the *fct*-Pt−Co@Pt/C exhibited outstanding mass activity that surpasses *fcc*-Pt−Co/C with an alloy phase, *fct*-Pt−Co/C with a truncated shape, and commercial Pt/C, by 5, 3, and 13 times, respectively.

Besides, a phase transformation of multiphasic heterostructures with well-defined shapes provides excellent opportunities to form intermetallic nanoarchitectures while preserving initial morphology. For example, the Tsung group demonstrated that the core/shell could transform into an intermetallic phase using a Pd/Ni/Pt multilayered core/shell nanocube as a self-template.[21] Within the multilayered core/shell, the intermixing between Ni and Pt layers occurs at elevated temperatures in well-controlled nanoscale geometries without external atomic diffusion. Increasing the Pt−Ni layer number or the thinning thickness of each layer can promote the intermixing, resulting in the atomic ordering at lower temperatures. In this synthesis, selecting the proper core materials was found to be vital to attain a highly ordered atomic arrangement in a well-defined shape. Core materials should direct the shape of the core/shell structure and serve as an inert platform for Pt−Ni intermixing process.

MULTIDIMENSIONAL INTERMETALLIC NANOSTRUCTURES

Next, we introduce recent examples of intermetallic nanoarchitectures with multidimensional nanostructures and their structural benefits and synthetic strategies. Due to their structural complexity, the formation of multidimensional intermetallic nanoarchitectures demands a more scrupulous effort than solid nanocrystals in zero-dimension (0D). The preparation methods developed for shape-defined intermetallic nanocrystals have been further improved to establish a general synthetic scheme of intermetallic nanoarchitectures having sophisticated dimensions. In particular, templating and protective layer coating methods have successfully produced multidimensional intermetallic nanoarchitecture from one-dimensional (1D) nanostructures to three-dimensional (3D) skeletal nanomaterials.[11,22−27,32]

1D nanomaterials, including NWs, nanorods, and nanotubes, have emerged as promising electrocatalytic nanostructures owing to their high surface-area-to-volume ratio and electrical conductivity. In addition, their anisotropy enables multiple contacts with the surface of the electrode or support materials,

https://doi.org/10.1021/acsnanoscienceau.2c00045
ACS Nanosci. Au XXXX, XXX, XXX−XXX

resulting in improved stability against aggregation of nanostructure or detachment from the electrode surface compared to the 0D nanocrystals. However, obtaining 1D nanostructures constructed with an intermetallic phase was not a trivial task.[6,9,10] When the external driving force is applied, the NWs often undergo a coarsening process to reduce their high surface energy. To address the shape deformation of NWs, Joo and co-workers exploited the thermally stable ordered mesoporous silica SBA-15, which serves as a template dictating NW structure with controlled diameters and as a protective layer against the coarsening of NWs.[11] Briefly, $H_2PtCl_6{\cdot}6H_2O$ and $CoCl_2{\cdot}6H_2O$ were impregnated into the SBA-15 and reduced at 300 °C to form alloy Pt_3Co NWs (*D*-Pt_3Co NWs). Before removing the SBA-15 template, the *D*-Pt_3Co NWs embedded in the SBA-15 were annealed at 600 °C to form intermetallic Pt_3Co NWs (*O*-Pt_3Co NWs) with face-centered cubic (*fcc*) crystal structure ($L1_2$ phase). After removing the SBA-15, two Pt_3Co NWs, which have nearly identical structural factors (size, shape, and dimension) but different internal atomic structures, were obtained. The resulting Pt_3Co NWs could serve as model catalytic systems for decoupling the impact of intermetallic structure from other factors. Theoretical calculations revealed that the ordered atomic arrangement in the intermetallic phase intensifies the ligand effect, fine-tuning the electronic structure of catalytic surfaces. It leads to higher catalytic activities of *O*-Pt_3Co NWs than *D*-Pt_3Co NWs toward multiple electrocatalytic reactions, including ORR, alkaline hydrogen evolution reaction (HER), and methanol oxidation reaction (MOR).

In another example, Zhang and co-workers developed intermetallic PtFeIr NWs possessing an *fct* crystal structure (*fct*-PtFeIr/C) with a diameter of 2.6 nm using silica protective layers.[22] To form silica protective layers on the catalyst, the as-prepared PtFeIr NWs with an alloy *fcc* phase (*fcc*-PtFeIr/C) was mixed with ethanol and ammonium hydroxide. Then, tetraethylorthosilicate (TEOS) was added to the mixture, and the mixture was stirred for 12 h. Finally, after the annealing process at 690 °C for 2 h and subsequent silica removal, the *fct*-PtFeIr/C was formed. In this synthesis, the silica protective layers assisted in preserving the initial sophisticated nanostructures during the high-temperature annealing process by suppressing coarsening of NWs. In the electrochemical tests, the *fct*-PtFeIr/C exhibited 1.8 and 9.7 times higher ORR mass activity than *fcc*-PtFeIr/C and commercial Pt/C catalysts, respectively. In addition, the *fct*-PtFeIr/C catalyst exhibited enhanced durability compared to the *fcc*-PtFeIr/C and commercial Pt/C catalysts, indicating the synergistic effect between intermetallic phase and NW morphology. The NW structure, which features a defective surface and anisotropic nature, enabled multiple contacts with carbon support, preventing agglomeration and particle detachment from the support materials, thereby improving stability.

The intermetallic NWs could also be obtained by providing external driving forces to overcome the energy barrier for phase transformation. Huang et al. developed ultrathin PdCu intermetallic NW networks (PdCu-B2 NWs) by applying constant current density (10 mA cm^{-2}) to the PdCu alloy nanowires (PdCu-A1 NWs) in a 0.5 M H_2SO_4 solution for 10 h at room temperature (Figure 4a).[23] After the electrochemical process, the initial interconnected NW structure was well-preserved. PdCu-B2 NWs showed a polycrystalline nature, which consists of intermetallic PdCu having typical *d*-spacings of B2 (110) plane (0.205 nm) and B2 (100) plane (0.289) at

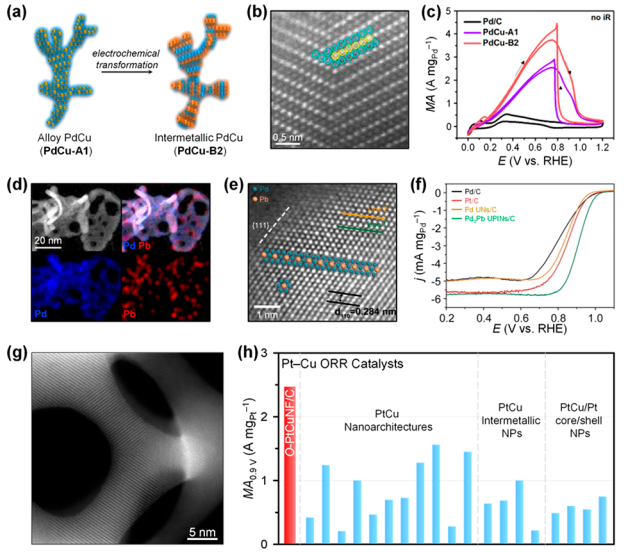

Figure 4. (a) Schematic illustration for the synthesis of PdCu-B2 NWs. (b) HAADF images of PdCu-B2 NWs showing area of twin defects at the tips of the ordered structure. Yellow circle indicates Pd, while blue circle indicates Cu. (c) FAOR CV curves of PdCu-B2 NWs, PdCu-A1 NWs, and Pd/C. Reprinted with permission from ref 23. Copyright 2020 American Chemical Society. (d) EDS elemental mapping data of Pd_3Pb UPINs. (e) HAADF-STEM image of Pd_3Pb UPINs showing an ordered atomic arrangement of Pd and Pb. (f) ORR polarization curves of Pd_3Pb UPINs/C, Pd UNs/C, Pt/C, and Pd/C. Reprinted with permission from ref 24. Copyright 2021 Wiley-VCH. (g) HAADF-STEM image of *O*-PtCuNF/C showing an ordered atomic arrangement of Pt and Cu. (h) Bar graph comparing the mass activities of *O*-PtCuNF/C and previously reported PtCu-based ORR catalysts. Reprinted with permission from ref 25. Copyright 2020 American Chemical Society.

the tips and junctions of interconnected NWs. Interestingly, the high-annular angle dark field (HAADF) STEM image of PdCu-B2 NWs indicated the twin boundaries that induce mismatches on their adjacent lattices (Figure 4b). The twin boundaries impose high compressive strain on the surface of PdCu-B2 NWs, leading to the modification of catalytic properties. Accordingly, the PdCu-B2 NWs showed high HER performance in 0.5 M H_2SO_4 with an overpotential of 19.7 mV at 10 mA cm^{-2}, which is smaller than monometallic Pd NWs (231.2 mV) and PdCu-A1 NWs (41.3 mV) catalysts and comparable to the commercial Pt/C (19.2 mV) catalyst. Moreover, PdCu-B2 NWs demonstrated excellence for the formic acid oxidation reaction (FAOR), where Pd-based catalysts are known to be the most optimal catalysts. PdCu-B2 NWs demonstrated the highest FAOR mass activity of 3.74 A mg_{Pd}^{-1} among all the studied materials, which is almost 7 times higher than the commercial Pd/C catalyst (Figure 4c).

A noticeable example exists for a two-dimensional (2D) intermetallic nanoarchitecture. Metallic nanosheets less than 10 atomic layers thick have attracted attention as efficient electrocatalysts owing to their high catalytic performance.[33] However, their inherent thin structure is vulnerable to agglomeration at high temperatures. To address this issue, Huang and co-workers synthesized Pd_3Pb ultrathin porous intermetallic nanosheets (UPINs) using Pd ultrathin nanosheets (UNs) as a template.[24] Typically, the Pd UN seeds with the average lateral size of 73.9 nm and thickness of 1.6 nm were mixed with OAm, $Pb(acac)_2$, and AA. Then, the mixture was heated at 140 °C for 10 min to form Pd_3Pb UPINs. The

https://doi.org/10.1021/acsnanoscienceau.2c00045
ACS Nanosci. Au XXXX, XXX, XXX−XXX

resulting Pd_3Pb UPINs exhibited 2D porous nanostructure, whose lateral size and thickness are 61.4 and 2.6 nm, respectively. The STEM-EDS elemental mapping showed even dispersion of Pd and Pb elements throughout the UPINs (Figure 4d). The atomic-resolution HAADF-STEM image proved the ordered Pd−Pb atomic arrangement, showing periodic brightness contrast (Figure 4e). In this synthesis, the structural evolution of UPINs was triggered by the incorporation of Pb atoms. At the early stage, Pd UNs underwent a deformation into a porous nanosheet morphology by the promoted oxidative etching at 140 °C. Then, the incorporated Pb atoms deposited on the defective sites of Pd UNs facilitated the Pd migration. Consequently, the accelerated Pd migration led to interatomic diffusion, disorder-to-order transformation, and pore evolution to form a highly porous 2D nanoarchitecture. Notably, this synthetic method was also applicable to prepare Pd_3Sn UPINs and PdCd UPINs by replacing secondary metal elements. In electrochemical assessment, the ORR activity of Pd_3Pb UPINs/C was evaluated along with Pd/C, Pt/C, and Pd UNs/C in 0.1 M KOH. The ORR activity was found to be in the order of Pd_3Pb UPINs/C > Pt/C > Pd UNs/C > Pd/C, indicating that the combination of intermetallic Pd_3Pb phase and UPIN structure induced the excellent ORR activity of Pd surface surpassing that of the Pt/C catalyst (Figure 4f). The UPIN structure that comprises abundant undercoordinated defects and curved planes provided energetic sites, boosting the intrinsic activity of the intermetallic Pd_3Pb surface. However, the examples of intermetallic nanosheets are very rare, pointing to the necessity to develop the rational synthetic strategy further for the 2D intermetallic structures.

Next, we present recent advances in 3D intermetallic nanoarchitectures.[25−27] The 3D skeletal nanomaterials, including nanoframes and nanocages, represent advanced electrocatalysts with a high surface-area-to-volume ratio.[34−36] In addition, the intrinsic catalytic activities of 3D nanostructures are much higher than 0D nanocrystals owing to the nanoscale confinement effect. As demonstrated by Stamenkovic and coworkers, these factors collectively increase the collision frequency of reactants, boosting catalytic activity.[36] However, their hollow structure is vulnerable to coarsening at elevated temperatures due to their inherently low stability. The aforementioned template-directed synthesis and protective layer-mediated annealing method were successfully applied to design highly crystalline intermetallic structures with sophisticated 3D nanoarchitectures. Joo, Lee, and co-workers developed, for the first time, the intermetallic PtCu rhombic dodecahedral nanoframes (*O*-PtCuNF/C) with the rhombohedral crystal structure ($L1_1$ phase) via protective layer-mediated annealing of alloy PtCu rhombic dodecahedral nanoframes (*D*-PtCuNF/C).[25] The as-prepared *D*-PtCuNF/C was mixed with TEOS and formic acid. Then, the mixture was dried to form silica protective layers on the *D*-PtCuNF/C. After annealing at 600 °C and subsequent silica etching, the *O*-PtuCuNF/C was obtained. Its HAADF-STEM image revealed the rhombic dodecahedral nanoframe structure constructed with a highly crystalline intermetallic PtCu phase (Figure 4g). In this synthesis, the silica protective layers assist in increasing crystallinity, in addition to suppressing the coarsening of the nanoframe structure. In the thermal treatment without silica coating, *D*-PtCuNF/C deformed into Pt−Cu spherical NPs with large particle size and a low intermetallic PtCu phase purity, revealing the nanoreactor role of the silica protective layer that promotes the disorder-to-order transformation. In the ORR electrocatalysis, the *O*-PtCuNF/C demonstrated superior ORR activity, durability, and chemical stability over the *D*-PtCuNF/C and Pt/C catalysts. Moreover, the *O*-PtCuNF/C delivered the highest ORR mass activity among PtCu-based catalysts, including PtCu/Pt core/shell NPs, PtCu intermetallic NPs, and alloy PtCu nanoarchitectures (Figure 4h). It clearly indicates that the intermetallic phase combined with the catalytic benefits of 3D nanoarchitectures, including curved planes, defects, lattice mismatch, and nanoscale confinement effect, yield high performance.

Recently, Liu and co-workers expanded the feasibility of the hard-templating method into the ordered mesoporous ternary intermetallic PtZnM (MI-PtZnM; M = Sc, V, Cr, Mn, Fe, Co, Ni, Cu, and Ga) catalysts with double-gyroid 3D network structure using KIT-6 mesoporous silica.[27] In this synthesis, the Zn atoms in binary intermetallic PtZn were substituted to form ternary PtZnM phases in the pores of KIT-6 templates. Briefly, as-prepared mesoporous intermetallic PtZn embedded in the KIT-6 (MI-PtZn/KIT-6) was mixed with M precursor solution and annealed at 500 °C for 6 h. After removing the silica template, the MI-PtZnM catalysts were obtained. The selective substitution of ordered MI-PtZn bimetals with M could optimize the electronic properties, leading to superior HER activity to binary MI-PtZn catalyst in various electrolyte media (1 M KOH, 1 M PBS, and 0.5 M H_2SO4). In addition, the best-performing MI-PtZnCo catalyst demonstrated excellent HER and stability in those electrolyte media. This result indicates that the compositional tuning of intermetallic nanoarchitectures can further boost catalytic performances.

CONCLUSION

In this Perspective, we categorized the structural factors of intermetallic nanoarchitectures that have improved electrocatalytic performance, including a high density of active sites, controlled facets, surface defects, strained surfaces, and nanoscale confinement effects. We also discussed diverse types of nanoarchitectures engineered to enhance the electrocatalytic performance of intermetallic phases, including facet-controlled nanocrystals and multidimensional nanostructures. In spite of the remarkable progress, the intermetallic nanoarchitectures have remaining challenges as follows: (i) demonstration of high-performance in the practical single-cells, (ii) understanding of electrocatalysis by intermetallic nanoarchitecture in terms of catalytic structure, and (iii) exploration of new synthetic approaches for a more facile intermetallic conversion.

For the widespread use of intermetallic nanoarchitectures, their excellent performances should be demonstrated in the single-cell configuration. Since most high-performance catalysts suffered from a degradation in their initial performance in single-cells due to stability issues, the intermetallic nanoarchitectures should be designed to endure the harsher condition of single-cells. Strengthening the interaction between intermetallic nanoarchitecture and support materials would be useful. The novel support materials that significantly influence electron transfer between two components can enable the full reflection of excellent catalytic properties of intermetallic nanoarchitecture at the practical device level by improving the electrochemical stability. For example, Liang et al. reported the synthesis of small PtCo intermetallic nanoparticles (PtCo-iNPs) via strong chemical interaction between Pt and S atoms in carbon support (Figure 5a).[37] Because S-doped carbon

https://doi.org/10.1021/acsnanoscienceau.2c00045
ACS Nanosci. Au XXXX, XXX, XXX−XXX

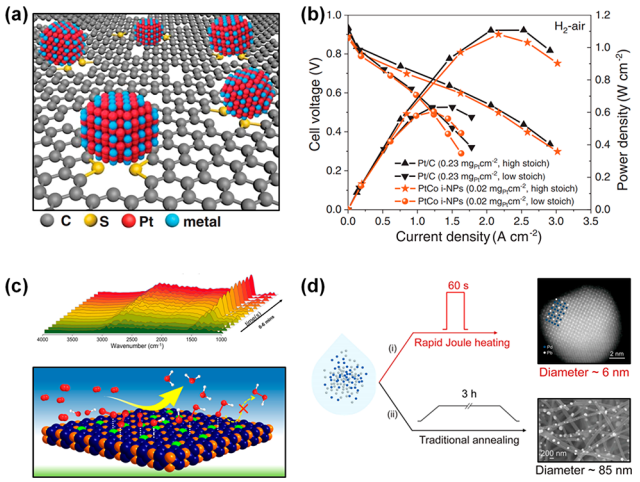

Figure 5. (a) Schematic illustration of Pt-based intermetallic nanoparticles anchoring on S-doped carbon with strong chemical interaction between nanocatalyst and carbon support. (b) H_2-air fuel cell polarization and power density curves with Pt/C and PtCo-iNPs as the cathode catalysts. Reprinted with permission from ref 37. Copyright 2021 American Association for the Advancement of Science. (c) Operando FTIR spectra and schematic illustration of intermetallic $Pt_{0.2}Pd_{1.8}Ge$ catalyst during the ORR. Reprinted with permission from ref 38. Copyright 2022 American Chemical Society. (d) Schematic illustration of two synthetic methods and HAADF-STEM and SEM images for resulting intermetallic Pd_3Pb nanoparticles prepared by each method: (i) rapid Joule heating method and (ii) traditional annealing method. Reprinted with permission from ref 39. Copyright 2022 American Chemical Society.

facilitates electron transfer and prevents disintegration and agglomeration of catalysts, the PtCo-iNPs could deliver high performance in practical PEMFCs, typically driven at elevated temperatures under radical-abundant environments. As shown in Figure 5b, the PtCo-iNPs with ultralow Pt loading (0.02 mg_{Pt} cm^{-2}) showed a similar catalytic performance to Pt/C with 11.5 times higher Pt loading (0.23 mg_{Pt} cm^{-2}) in an H_2-air PEMFC test.

Comprehending the mechanisms for the electrochemical reactions catalyzed by intermetallic nanoarchitectures is also crucial. However, we have a poor understanding of the role of respective structural factors and composition in performance enhancement by intermetallic nanoarchitecture. An in-depth operando analysis can reveal the reaction mechanism on the surface of intermetallic phases and guide the proper composition and structures of new intermetallic nanoarchitectures. For examples, Peter et al. conducted operando Fourier transform infrared (FTIR) spectroscopy and computational studies to reveal reaction mechanisms of water formation during the ORR (Figure 5c).[38] They observed changes in the structure and reaction kinetics of the intermetallic $Pt_{0.2}Pd_{1.8}Ge$ catalyst during electrocatalytic reactions and confirmed that inhibition of OH* poisoning was induced by weaker OH* adsorption and stronger OOH* adsorption. In situ characterization techniques such as X-ray photoelectron spectroscopy, X-ray absorption fine structure spectroscopy, and inductive coupled plasma mass spectroscopy are also anticipated to be helpful to further improvement in catalytic properties of the intermetallic nanoarchitectures.

Furthermore, it is necessary to develop robust synthetic strategies employing mild conditions at low temperatures and straightforward processes to adopt intermetallic nanoarchitectures extensively. Synthesis of intermetallic nanoarchitectures still remains a critical challenge because the disorder-to-order transformation is usually conducted at high temperatures for a long time. In particular, the synthesis of intermetallic nanoarchitecture should be performed very carefully due to their higher surface energy than simple intermetallic NPs. Even though the wet-chemical approaches enabled the low-temperature synthesis of intermetallic nanoarchitectures, the large-scale synthesis is very cumbersome. Thus, a simple process facilitating atom migration for generating the intermetallic phases represents a breakthrough in the synthesis of intermetallic nanoarchitectures. The recently reported rapid Joule heating method (Figure 5d) can be a viable solution, producing intermetallic Pd_3Pb NPs in 60 s by increasing the vacancy concentration or mixing low-melting point elements.[39] By combining the aforementioned templating methods, this method can serve as a new design strategy for intermetallic nanostructures with a simple process.

As discussed herein, intermetallic nanoarchitectures exhibit great potential in practical devices for electrochemical energy conversion systems owing to their high intrinsic activity, stability, and selectivity. We hope that this Perspective suggests a direction for the future design of electrocatalysts that accelerate the widespread use of energy conversion systems.

AUTHOR INFORMATION

Corresponding Authors

Sang Hoon Joo − *Department of Chemistry, Ulsan National Institute of Science and Technology (UNIST), Ulsan 44919, Republic of Korea;* orcid.org/0000-0002-8941-9662; Email: shjoo@unist.ac.kr

Kwangyeol Lee − *Department of Chemistry and Research Institute for Natural Science, Korea University, Seoul 02841, Republic of Korea;* orcid.org/0000-0003-0575-7216; Email: kylee1@korea.ac.kr

Authors

Ho Young Kim − *Hydrogen·Fuel Cell Research Center, Korea Institute of Science and Technology (KIST), Seoul 02792, Republic of Korea;* orcid.org/0000-0002-9560-192X

Minki Jun − *Department of Chemistry and Research Institute for Natural Science, Korea University, Seoul 02841, Republic of Korea;* orcid.org/0000-0002-4592-4819

Complete contact information is available at: https://pubs.acs.org/10.1021/acsnanoscienceau.2c00045

Author Contributions

#H.Y.K. and M.J. contributed equally. CRediT: **Ho Young Kim** writing-original draft (lead); **Minki Jun** writing-original draft (equal); **Sang Hoon Joo** supervision (equal), writing-review & editing (equal); **Kwangyeol Lee** supervision (lead), writing-review & editing (lead).

Notes

The authors declare no competing financial interest.

ACKNOWLEDGMENTS

This work was supported by the National Research Foundation (NRF) of Korea funded by the Ministry of Science and ICT (NRF-2019R1A6A1A11044070 and NRF-2021M3H4A1A02049916 to K.L.; NRF-2019M3E6A1064521, NRF-2019M3D1A1079306, NRF-2019M1A2A2065614, and

https://doi.org/10.1021/acsnanoscienceau.2c00045
ACS Nanosci. Au XXXX, XXX, XXX−XXX

NRF-2021R1A2C2007495 to S.H.J.). K.L. also acknowledges the support of Korea Institute of Energy Technology Evaluation and Planning (KETEP) grant (Grant No. 20203020030010). H.Y.K. acknowledges the support of KIST Institutional Program (Project No. 2E32149).

REFERENCES

(1) Gray, H. B. Powering the Planet with Solar Fuel. *Nat. Chem.* **2009**, *1*, 7.
(2) Chu, S.; Majumdar, A. Opportunities and Challenges for a Sustainable Energy Future. *Nature* **2012**, *488*, 294−303.
(3) Jiao, Y.; Zheng, Y.; Jaroniec, M. T.; Qiao, S. Z. Design of Electrocatalysts for Oxygen- and Hydrogen-Involving Energy Conversion Reactions. *Chem. Soc. Rev.* **2015**, *44*, 2060−2086.
(4) Seh, Z. W.; Kibsgaard, J.; Dickens, C. F.; Chorkendorff, I.; Norskov, J. K.; Jaramillo, T. F. Combining Theory and Experiment in Electrocatalysis: Insights into Materials Design. *Science* **2017**, *355*, No. eaad4998.
(5) Xia, Y.; Yang, X. Toward Cost-Effective and Sustainable Use of Precious Metals in Heterogeneous Catalysts. *Acc. Chem. Res.* **2017**, *50*, 450−454.
(6) Yan, Y.; Du, J. S.; Gilroy, K. D.; Yang, D.; Xia, Y.; Zhang, H. Intermetallic Nanocrystals: Syntheses and Catalytic Applications. *Adv. Mater.* **2017**, *29*, 1605997.
(7) Furukawa, S.; Komatsu, T. Intermetallic Compounds: Promising Inorganic Materials for Well-Structured and Electronically Modified Reaction Environments for Efficient Catalysis. *ACS Catal.* **2017**, *7*, 735−765.
(8) Rößner, L.; Armbrüster, M. Electrochemical Energy Conversion on Intermetallic Compounds: A Review. *ACS Catal.* **2019**, *9*, 2018−2062.
(9) Kim, H. Y.; Joo, S. H. Recent Advances in Nanostructured Intermetallic Electrocatalysts for Renewable Energy Conversion Reactions. *J. Mater. Chem. A* **2020**, *8*, 8195−8217.
(10) Williams, B. P.; Qi, Z.; Huang, W.; Tsung, C. K. The Impact of Synthetic Method on the Catalytic Application of Intermetallic Nanoparticles. *Nanoscale* **2020**, *12*, 18545−18562.
(11) Kim, H. Y.; Kim, J. M.; Ha, Y.; Woo, J.; Byun, A.; Shin, T. J.; Park, K. H.; Jeong, H. Y.; Kim, H.; Kim, J. Y.; Joo, S. H. Activity Origin and Multifunctionality of Pt-Based Intermetallic Nanostructures for Efficient Electrocatalysis. *ACS Catal.* **2019**, *9*, 11242−11254.
(12) Watanabe, M.; Tsurumi, K.; Mizukami, T.; Nakamura, T.; Stonehart, P. Activity and Stability of Ordered and Disordered Co−Pt Alloys for Phosphoric Acid Fuel Cells. *J. Electrochem. Soc.* **1994**, *141*, 2659−2668.
(13) Ji, X. L.; Lee, K. T.; Holden, R.; Zhang, L.; Zhang, J. J.; Botton, G.; Couillard, M.; Nazar, L. Nanocrystalline Intermetallics on Mesoporous Carbon for Direct Formic Acid Fuel Cell Anodes. *Nat. Chem.* **2010**, *2*, 286−293.
(14) Wang, D.; Xin, H. L.; Hovden, R.; Wang, H.; Yu, Y.; Muller, D. A.; DiSalvo, F. J.; Abruña, H. D. Structurally Ordered Intermetallic Platinum−Cobalt Core−Shell Nanoparticles with Enhanced Activity and Stability as Oxygen Reduction Electrocatalysts. *Nat. Mater.* **2013**, *12*, 81−87.
(15) Li, Q.; Wu, L.; Wu, G.; Su, D.; Lv, H.; Zhang, S.; Zhu, W.; Casimir, A.; Zhu, H.; Mendoza-Garcia, A.; Sun, S. New Approach to Fully Ordered fct-FePt Nanoparticles for Much Enhanced Electrocatalysis in Acid. *Nano Lett.* **2015**, *15*, 2468−2473.
(16) Chung, D. Y.; Jun, S. W.; Yoon, G.; Kwon, S. G.; Shin, D. Y.; Seo, P.; Yoo, J. M.; Shin, H.; Chung, Y.-H.; Kim, H.; Mun, B. S.; Lee, K.-S.; Lee, N.-S.; Yoo, S. J.; Lim, D.-H.; Kang, K.; Sung, Y.-E.; Hyeon, T. Highly Durable and Active PtFe Nanocatalyst for Electrochemical Oxygen Reduction Reaction. *J. Am. Chem. Soc.* **2015**, *137*, 15478−15485.
(17) Qi, Z.; Xiao, C.; Liu, C.; Goh, T. W.; Zhou, L.; Maligal-Ganesh, R.; Pei, Y.; Li, X.; Curtiss, L. A.; Huang, W. Sub-4 nm PtZn Intermetallic Nanoparticles for Enhanced Mass and Specific Activities in Catalytic Electrooxidation Reaction. *J. Am. Chem. Soc.* **2017**, *139*, 4762−4768.
(18) Bu, L.; Zhang, N.; Guo, S.; Zhang, X.; Li, J.; Yao, J.; Wu, T.; Lu, G.; Ma, J.-Y.; Su, D.; Huang, X. Biaxially Strained PtPb/Pt Core/Shell Nanoplate Boosts Oxygen Reduction Catalysis. *Science* **2016**, *354*, 1410−1414.
(19) Gao, Q.; Pillai, H. S.; Huang, Y.; Liu, S.; Mu, Q.; Han, X.; Yan, Z.; Zhou, H.; He, Q.; Xin, H.; Zhu, H. Breaking Adsorption-Energy Scaling Limitations of Electrocatalytic Nitrate Reduction on Intermetallic CuPd Nanocubes by Machine-Learned Insights. *Nat. Commun.* **2022**, *13*, 2338.
(20) Xie, M.; Lyu, Z.; Chen, R.; Shen, M.; Cao, Z.; Xia, Y. Pt-Co@Pt Octahedral Nanocrystals: Enhancing Their Activity and Durability Toward Oxygen Reduction with an Intermetallic Core and an Ultrathin Shell. *J. Am. Chem. Soc.* **2021**, *143*, 8509−8518.
(21) Williams, B. P.; Young, A. P.; Andoni, I.; Han, Y.; Lo, W.-S.; Golden, M.; Yang, J.; Lyu, L.-M.; Kuo, C.-H.; Evans, J. W.; Huang, W.; Tsung, C.-K. Strain-Enhanced Metallic Intermixing in Shape-Controlled Multilayered Core-Shell Nanostructures: Toward Shaped Intermetallics. *Angew. Chem., Int. Ed* **2020**, *59*, 10574−10580.
(22) Yang, Z.; Yang, H.; Shang, L.; Zhang, T. Ordered PtFeIr Intermetallic Nanowires Prepared through a Silica-Protection Strategy for the Oxygen Reduction Reaction. *Angew. Chem., Int. Ed* **2022**, *61*, No. e202113278.
(23) Flores Espinosa, M. M.; Cheng, T.; Xu, M.; Abatemarco, L.; Choi, C.; Pan, X.; Goddard, W. A.; Zhao, Z.; Huang, Y. Compressed Intermetallic PdCu for Enhanced Electrocatalysis. *ACS Energy Lett.* **2020**, *5*, 3672−3680.
(24) Guo, J.; Gao, L.; Tan, X.; Yuan, Y.; Kim, J.; Wang, Y.; Wang, H.; Zeng, Y. J.; Choi, S.-I.; Smith, S. C.; Huang, H. Template-Directed Rapid Synthesis of Pd-Based Ultrathin Porous Intermetallic Nanosheets for Efficient Oxygen Reduction. *Angew. Chem., Int. Ed* **2021**, *60*, 10942−10949.
(25) Kim, H. Y.; Kwon, T.; Ha, Y.; Jun, M.; Baik, H.; Jeong, H.; Kim, H.; Lee, K.; Joo, S. H. Intermetallic PtCu Nanoframes as Efficient Oxygen Reduction Electrocatalysts. *Nano Lett.* **2020**, *20*, 7413−7421.
(26) Yang, X.; Yao, K. x.; Ye, J. Y.; Yuan, Q.; Zhao, F.; Li, Y.; Zhou, Z. Interface-Rich Three-Dimensional Au-Doped PtBi Intermetallics as Highly Effective Anode Catalysts for Application in Alkaline Ethylene Glycol Fuel Cells. *Adv. Funct. Mater.* **2021**, *31*, 2103671.
(27) Wang, Y.; Lv, H.; Sun, L.; Jia, F.; Liu, B. Ordered Mesoporous Intermetallic Trimetals for Efficient and pH-Universal Hydrogen Evolution Electrocatalysis. *Adv. Energy Mater.* **2022**, *12*, 2201478.
(28) An, K.; Somorjai, G. A. Size and Shape Control of Metal Nanoparticles for Reaction Selectivity in Catalysis. *ChemCatChem.* **2012**, *4*, 1512−1524.
(29) Cao, S.; Tao, F.; Tang, Y.; Li, Y.; Yu, J. Size- and Shape-Dependent Catalytic Performances of Oxidation and Reduction Reactions on Nanocatalysts. *Chem. Soc. Rev.* **2016**, *45*, 4747−4765.
(30) Jia, Y.; Jiang, K.; Wang, H.; Yao, X. The Role of Defect Sites in Nanomaterials for Electrocatalytic Energy Conversion. *Chem.* **2019**, *5*, 1371−1397.
(31) Xie, C.; Yan, D.; Chen, W.; Zou, Y.; Chen, R.; Zang, S.; Wang, Y.; Yao, X.; Wang, S. Insight into the Design of Defect Electrocatalysts: From Electronic Structure to Adsorption Energy. *Mater. Today* **2019**, *31*, 47−68.
(32) Baek, D. S.; Joo, S. H. Non-Siliceous Ordered Mesoporous Materials via Nanocasting for Small Molecule Conversion Electrocatalysis *Bull. Korean Chem. Soc.*. **2022**, *431156* (accessed 2022−10−20).
(33) Ranjan, P.; Gaur, S.; Yadav, H.; Urgunde, A. B.; Singh, V.; Patel, A.; Vishwakarma, K.; Kalirawana, D.; Gupta, R.; Kumar, P. 2D Materials: Increscent Quantum Flatland with Immense Potential for Applications. *Nano Convergence* **2022**, *9*, 26.
(34) Park, J.; Kwon, T.; Kim, J.; Jin, H.; Kim, H. Y.; Kim, B.; Joo, S. H.; Lee, K. Hollow Nanoparticles as Emerging Electrocatalysts for Renewable Energy Conversion Reactions. *Chem. Soc. Rev.* **2018**, *47*, 8173−8202.

https://doi.org/10.1021/acsnanoscienceau.2c00045
ACS Nanosci. Au XXXX, XXX, XXX−XXX

(35) Kwon, T.; Jun, M.; Lee, K. Catalytic Nanoframes and Beyond. *Adv. Mater.* **2020**, *32*, 2001345.
(36) Chen, C.; Kang, Y.; Huo, Z.; Zhu, Z.; Huang, W.; Xin, H. L.; Snyder, J. D.; Li, D.; Herron, J. A.; Mavrikakis, M.; Chi, M.; More, K. L.; Li, Y.; Markovic, N. M.; Somorjai, G. A.; Yang, P.; Stamenkovic, V. R. Highly Crystalline Multimetallic Nanoframes with Three-Dimensional Electrocatalytic Surfaces. *Science* **2014**, *343*, 1339−1343.
(37) Yang, C.-L.; Wang, L.-N.; Yin, P.; Liu, J.; Chen, M.-X.; Yan, Q.-Q.; Wang, Z.-S.; Xu, S.-L.; Chu, S.-Q.; Cui, C.; Ju, H.; Zhu, J.; Lin, Y.; Shui, J.; Liang, H.-W. Sulfur-Anchoring Synthesis of Platinum Intermetallic Nanoparticle Catalysts for Fuel Cells. *Science* **2021**, *374*, 459−464.
(38) Mondal, S.; Bagchi, D.; Riyaz, M.; Sarkar, S.; Singh, A. K.; Vinod, C. P.; Peter, S. C. In Situ Mechanistic Insights for the Oxygen Reduction Reaction in Chemically Modulated Ordered Intermetallic Catalyst Promoting Complete Electron Transfer. *J. Am. Chem. Soc.* **2022**, *144*, 11859−11869.
(39) Cui, M.; Yang, C.; Hwang, S.; Li, B.; Dong, Q.; Wu, M.; Xie, H.; Wang, X.; Wang, G.; Hu, L. Rapid Atomic Ordering Transformation toward Intermetallic Nanoparticles. *Nano Lett.* **2022**, *22*, 255−262.

https://doi.org/10.1021/acsnanoscienceau.2c00045
ACS Nanosci. Au XXXX, XXX, XXX−XXX